On the new mode of instability in high-speed boundary layer flows

Jie Ren

School of aerospace engineering
Tsinghua University
Beijing, China
jieren@tsinghua.edu.cn

Youcheng Xi

School of aerospace engineering
Tsinghua University
Beijing, China
xiyc14@mails.tsinghua.edu.cn

Song Fu

School of aerospace engineering
Tsinghua University
Beijing, China
fs-dem@tsinghua.edu.cn

ABSTRACT

The new mode of instability found by Tunney *et al.* (2015) is studied with viscous stability theory in this article. When the high-speed boundary layer is subjected to certain values of favorable pressure gradient and wall heating, a new mode becomes unstable due to the appearance of the streamwise velocity overshoot ($U(y) > U_\infty$) in the base flow. The present study shows that the new mode can hardly coexist with conventional first mode and Mack's second mode, however, may lead to the transition of new scenarios.

1 Introduction

The mechanism of high-speed laminar-turbulent flow transition is far from fully understood (Fedorov, 2011). One important reason is the diverse routes of the transition process that is in turn influenced by multifarious environmental conditions. Among them, modal stability is generally considered the fundamental mechanism and relatively well-studied. The representative examples are Tollmien-Schlichting waves in (quasi-) parallel flows (Schlichting & Gersten, 2017), Mack's second modes in hypersonic flows (Mack, 1984), cross-flow modes in three-dimensional boundary layers (Saric *et al.*, 2003) and Görtler modes over concave surfaces (when Reynolds number is large) (Saric, 1994). Under certain conditions, perturbations (generated through receptivity mechanism) get amplified with modal instabilities causing the flow close to transition when their amplitude becomes large. However, even after amounts of studies, the knowledge on this fundamental modal stability is still insufficient.

Compared with zero pressure gradient, favorable pressure gradient (hereafter referred to as FPG) significantly stabilizes the boundary layer in both incompressible and compressible flows (the first mode as well as Mack's second mode). This is supported by a number of studies, e.g., with direct numerical simulation (Kloker & Fasel, 1990; Bech *et al.*, 1998; Franko & Lele, 2014), linear stability theory (Malik, 1989; Zurigat *et al.*, 1992; Masad & Zurigat, 1994) and very recent experiments (Tokugawa *et al.*, 2015; Costantini *et al.*, 2016). Hence, in the review by Reed *et al.* (1996), the instability of boundary layer with FPG is described as "*very weak, if it exists at all*". In fact, with FPG, the profile of the base flow $U(y)$ becomes fuller and the thickness of the boundary layer is decreased. This is mainly responsible for the stabilization of the boundary layer.

On the other hand, wall-heating/cooling is one of the common passive flow control methods used on various occasions. Its influence on boundary layer stability has been well documented (see reviews by Mack, 1987; Reed *et al.*, 1996). In contrast to the adiabatic condition, wall heating can destabilize the first mode while stabilizing Mack's second mode. Wall cooling, instead, has opposite effects. One shall distinguish between wall-heating and localized wall-heating. The latter gives rise to wall temperature jump effect and can destabilize Mack's second mode (see recent analysis by Fedorov *et al.*, 2015).

When the flow is subjected to the dual effects of FPG and wall-heating, a new mode comes to light. A first analytical study was performed by Tunney *et al.* (2015) under inviscid equations. The straight reason of the instability is the development of streamwise velocity *overshoot* ($U(y) > U_\infty$ near the upper edge of the boundary layer). Discussion on the *overshoot* can be found in Tunney *et al.* (2015) and the references therein. Under inviscid assumption, the new mode was shown to have comparable growth rate as the conventional first mode and Mack's higher mode. Therefore, the new mode is of primary importance in hypersonic flow transition.

In this paper, we report a viscous stability analysis on this new mode. In Section 2 the methodology and the base flow are introduced. Modal stability is discussed in Section 3, and the paper is concluded in Section 4.

2 Methodology and base flow

The stability equations are derived from the Navier-Stokes equations provided the base flow is obtained in advance. A frequently-adopted form is written as

$$\begin{aligned}&\Gamma\frac{\partial\tilde{q}}{\partial t}+A\frac{\partial\tilde{q}}{\partial x}+B\frac{\partial\tilde{q}}{\partial y}+C\frac{\partial\tilde{q}}{\partial z}+D\tilde{q}\\&=V_{xx}\frac{\partial^2\tilde{q}}{\partial x^2}+V_{xy}\frac{\partial^2\tilde{q}}{\partial x\partial y}+V_{xz}\frac{\partial^2\tilde{q}}{\partial x\partial z}+V_{yy}\frac{\partial^2\tilde{q}}{\partial y^2}+V_{yz}\frac{\partial^2\tilde{q}}{\partial y\partial z}+V_{zz}\frac{\partial^2\tilde{q}}{\partial z^2}.\end{aligned}\tag{1}$$

Here $\tilde{q}=(\tilde{\rho},\tilde{u},\tilde{v},\tilde{w},\tilde{T})^T$ is the perturbation vector of flow density, velocity and temperature. The 5×5 matrices Γ, A, B... are functions of the base flow and dimensionless parameters Re, Ma, Pr. Detailed expressions for these matrices can be found in the authors' previous articles (Ren & Fu, 2014, 2015). The physical quantities are nondimensionalized with their corresponding free-stream values except pressure p^* by $\rho^*_\infty U^{*2}_\infty$. Asterisk denotes dimensional quantities. The orthogonal coordinates x^*, y^*, z^* describing the distance

in streamwise, normalwise and spanwise directions are normalised with the length scale $\delta^* = \sqrt{\nu_\infty^* x^* / U_\infty^*}$. As a result, the dimensionless parameters Re, Ma, Pr are

$$Re = \frac{\rho_\infty^* U_\infty^* \delta^*}{\mu_\infty^*}, \quad Ma = \frac{U_\infty^*}{\sqrt{\gamma R_{air}^* T_\infty^*}}, \quad Pr = \frac{\mu_\infty^* C_p^*}{\kappa_\infty^*}. \tag{2}$$

One is able to identify, Re is a measure of streamwise coordinate when the freestream parameters are fixed. On the other hand, when $Re \to \infty$, the equations reduce to inviscid O-S and Squire equations in compressible form. In the framework of modal stability, equation (1) is solved as an eigenvalue problem through

$$\tilde{q}(x,y,z,t) = \hat{q}(y)\exp(i\alpha x + i\beta z - i\omega t) + c.c. \tag{3}$$

We focus on the spatial problem which is more relevant to practical boundary layer flows. Therefore, α is the eigenvalue to be numerically solved. In the above formulation, we have assumed the flow to be calorically-perfect-gas and Pr is constant. Therefore,

$$p^* = \rho^* R_{air}^* T^*, \ \gamma = 1.4, \ C_p^* = \text{const}, \ R_{air}^* = \text{const}, \ Pr = 0.72 = \text{const}. \tag{4}$$

The first coefficient of viscosity μ is given by Sutherland's law and the second coefficient follows Stokes's hypothesis, i.e., $\lambda = -2/3\mu$.

The similar solution of the boundary layer equations offers a concise thus normalised base flow. For a better understanding of the new mode and generation of the full stability diagram, it is employed in this study. Introducing the Mangler-Levy-Lees transformation (see detailed introduction in Schlichting & Gersten, 2017; Cebeci & Smith, 1974; Cebeci, 2002)

$$\left.\begin{aligned} \mathrm{d}\xi &= \rho_e \mu_e u_e \, \mathrm{d}x \\ \mathrm{d}\eta &= \frac{\rho u_e}{\sqrt{2\xi}} \, \mathrm{d}y \end{aligned}\right\} \tag{5}$$

into the boundary layer equations, yields the transformed equations:

$$\left.\begin{aligned} (cf'')' + ff'' + \beta_p(1+k)(g - f'^2) = 0 \\ (a_1 g' + a_2 f' f'')' + fg' = 0 \end{aligned}\right\} \tag{6}$$

where the prime denotes the derivative with respect to η. The coefficients are defined as

$$c = \frac{\mu}{T}, \quad a_1 = \frac{c}{Pr}, \quad a_2 = \frac{2k}{k+1}\left(1 - \frac{1}{Pr}\right)c, \quad k = \frac{(\gamma-1)}{2}Ma^2, \quad \beta_p = \frac{2\xi}{u_e}\frac{\mathrm{d}u_e}{\mathrm{d}\xi}. \tag{7a-e}$$

The physical quantities are recovered through

$$\frac{u^*}{u_\infty^*} = f', \quad \frac{H^*}{H_\infty^*} = g, \quad \frac{T^*}{T_\infty^*} = (1+k)g - kf'^2. \tag{8a-c}$$

Here H denotes the total enthalpy. It should be noted that the temperature-based energy equation is also frequently used. With the same transformation (5), the temperature-based energy equation becomes

$$\frac{1}{Pr}(c\theta')' + f\theta' + (\gamma-1)Ma^2 c f''^2 = 0, \tag{9}$$

where

$$\frac{T^*}{T_\infty^*} = \theta. \tag{10}$$

(6) or (9) can be solved with standard boundary value problem (BVP) solvers. The boundary conditions (isothermal) are

$$f(0) = f'(0) = 0, \quad g(0) = H_w, \quad f'(\infty) = g(\infty) = 1 \tag{11a-c}$$

and

$$f(0) = f'(0) = 0, \quad \theta(0) = T_w, \quad f'(\infty) = \theta(\infty) = 1. \tag{12a-c}$$

When $g'(0) = 0$ or $\theta'(0) = 0$ is applied instead of the Dirichlet condition, the flow is adiabatic.

Figure 1 shows the profiles of streamwise velocity and temperature. As can be observed, perfect matches with Tunney *et al.* (2015, with Chapman's law) and temperature based energy equation (see also Ricco *et al.*, 2009, with Sutherland's law) have been achieved. Along with the increase of the pressure gradient β_p, the laminar boundary layer profile $U(y)$ is essentially modified. The boundary layer thickness decreases. An inflection point appears along with the presence of the streamwise velocity overshoot (larger than the free-stream value).

3 Stability analysis

Three group of cases have been studied to reveal the stability diagram of the new mode and its relationship to conventional first and Mack's second mode. See Table 1 for the prescribed parameters. Case 1 serves as a basic case to recover the typical zero-pressure gradient boundary layer with adiabatic boundary condition. Wall heating is included in Case 2 and the dual effects of wall heating and FPG is considered in Case 3. A broad range of parameters is specified to show all the possible modal instabilities thus allowing a complete stability diagram.

Table 1. Parameters of the three cases studied. Mach number $Ma = 4.5$, Stagnation temperature $T_0^* = 329K$, Spanwise wavenumber $0 \leqslant \beta \leqslant 1$, angular frequency $0 \leqslant \omega \leqslant 1.2$ and Reynolds number $100 \leqslant Re \leqslant 2000$.

Case	Wall heating	Pressure gradient
1	$H_w' = 0$	$\beta_p = 0$
2	$H_w = 1.5$	$\beta_p = 0$
3	$H_w = 1.5$	$\beta_p = 0.4$

Figure 2(a) shows the stability diagram of zero-pressure gradient boundary layer subjected to adiabatic boundary conditions (Case 1). The unstable block (in the $Re - \beta - \omega$ space) of the first and second modes are enclosed by the corresponding enveloping surfaces. Apparently, both modes become unstable starting from certain Re numbers. These numbers, termed critical Reynolds numbers, indicate that the perturbations gain exponential eigen-growth downstream of the leading edge. As can be seen from Figure 2(a),

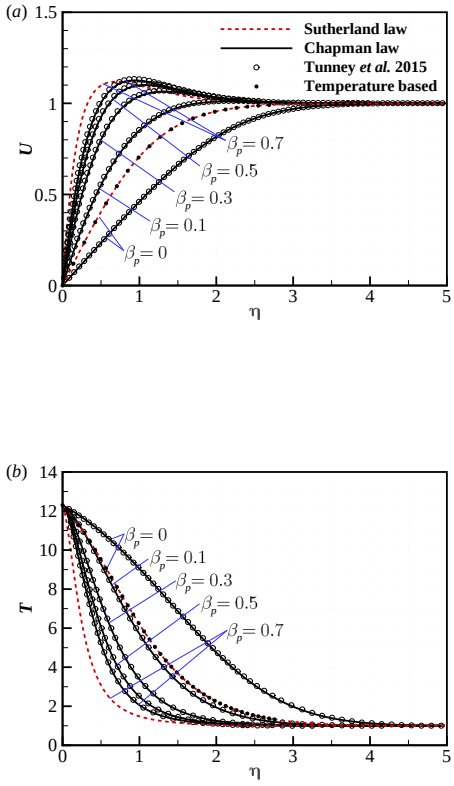

Figure 1. Profiles of (a) the streamwise velocity U and (b) temperature T as functions of the similarity variable η. The Falkner-Skan pressure gradient parameter $\beta_p = 0,\ 0.1,\ 0.3,\ 0.5$ and 0.7 respectively. $Ma = 6$, $H_w = 1.5$ and $Pr = 0.72$.

the unstable regions of the two modes do not intersect with each other at $Ma = 4.5$. The angular frequency of the second mode is above the first mode, therefore possessing a higher frequency.

Several surface cuts are shown with $\beta = 0,\ 0.04,\ 0.08,\ 0.12,\ 0.16$ and 0.20 respectively. These iso-surfaces show contours of the eigenvalue α_i ($-\alpha_i$ is the local growth rate). One can see that the second mode have an obviously larger growth rate and it reaches maximum growth rate at $\beta = 0$. When β is increased, both the maximum growth rate and the unstable area get reduced. As a result, it is generally accepted that the 2-D perturbation ($\beta = 0$) is the most dangerous for the second mode. On the other hand, the optimal spanwise wavenumber for the first mode is not zero.

When wall-heating is imposed, as shown in Figure 2(b), Mack's second mode is significantly stabilized. Both the maximum growth rate and the unstable area become reduced. On the other hand, the first mode is enhanced. The maximum growth rate is not much increased but the unstable region is expanded to a major degree, intruding into Mack's second mode.

As can be seen in Figure 2(c), with the dual effects of wall-heating and FPG, the new mode becomes the only unstable mode in the boundary layer. By comparing with Case 1 and Case 2, the new mode has a much larger unstable region in terms of β and ω. Interestingly, it reaches maximum growth rate at $\beta = 0$ but has smaller growth rate compared with the conventional modes. Case 2 and 3 are plotted together in Figure 2(d). It is apparent that the new mode

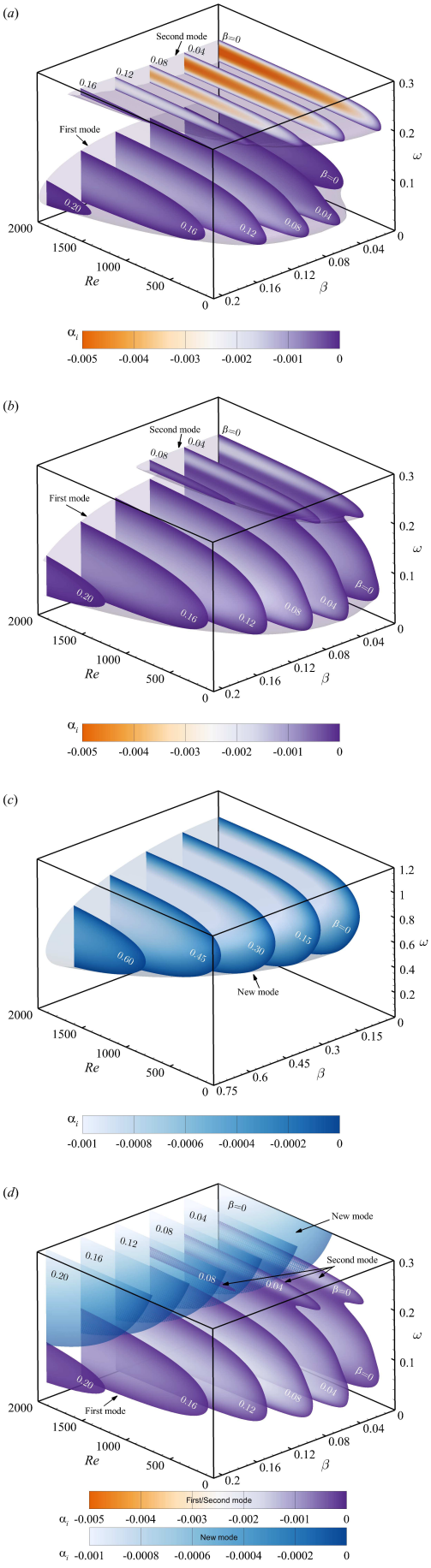

Figure 2. Stability diagram of the boundary layer for Case 1 (a); Case 2 (b); Case 3 (c); Case 2 & 3 (d).

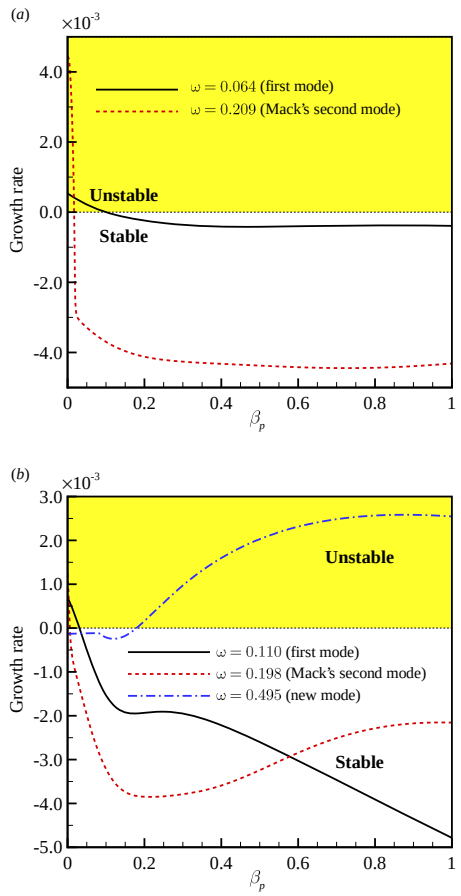

Figure 3. Growth rate of 2-D perturbations ($\beta = 0$) as functions of pressure gradient β_p. (a) Boundary layer with adiabatic condition (H'_w=0); (b) Boundary layer with wall-heating (H_w=1.5);

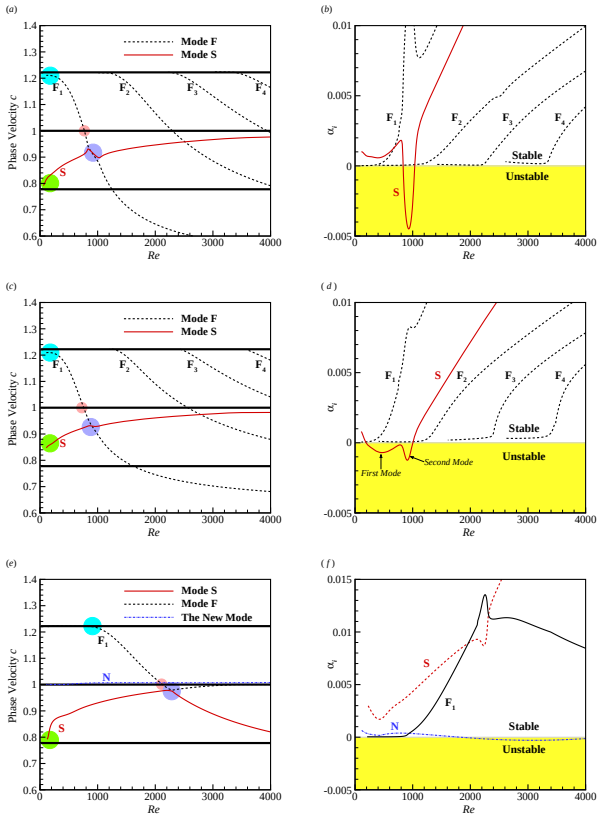

Figure 4. Spectrum of the 2-D perturbations ($\beta = 0$) with frequency $F = \omega/Re = 2.2 \times 10^{-4}$ for Case 1 (a,b); Case 2 (c,d) and Case 3 (e,f). The thick horizontal lines (in a,c,e) show the phase velocities of the continuous spectrum: fast acoustic wave ($c = 1 + 1/Ma$=1.22), voticity/entropy wave ($c = 1.0$) and slow acoustic wave ($c = 1 - 1/Ma$=0.78). The solid circles show the synchronization regions. The notations F_1, F_2... represent the multiple Fast mode excited consecutively.

covers the frequency band of the Mack's second mode and extends to much higher values.

It is remarkable that the new mode becomes the only unstable modes when dual effects (wall-heating and FPG) are present. This is interpreted in Figure 3 where the influence of pressure gradient β_p is revealed. Several representative frequencies were chosen to show the possible unstable modes. The results show that, whether the wall is heated or adiabatic, it does not change the significant stabilizing effect of FPG on the conventional modes. Both the first mode and Mack's second mode soon become stable when FPG increases to $\beta_p = 0.1$. Mack's second mode is even more sensitive to this parameter. This is consistent with previous studies as introduced in Section 1. On the other hand, the new mode starts growing when β_p reaches a value of about 0.2. Hence, the new mode becomes the only unstable mode in boundary layer with FPG & wall-heating.

The spectrum of high-speed boundary layers has been shown (see reviews by Fedorov, 2011; Zhong & Wang, 2012) to help the understanding of the excitation of the unstable modes. The synchronization between Mode F (stems from the fast acoustic wave) and Mode S (stems from the slow acoustic wave) gives rise to the growth of Mack's second mode. Detailed comments on the synchronization were made by Federov & Tumin (2011). Figure 4 shows the discrete spectrum (phase velocity $c = \omega/\alpha_r$ and imaginary part of the eigenvalue α_i.) for the three cases at fixed physical frequency $F = \omega/Re = 2.2 \times 10^{-4}$.

Case 1 reproduced the spectrum in conventional adiabatic boundary layers with zero pressure gradient. At this frequency, Mode S played the first mode and Mack's second mode at different sections of Reynolds numbers. The first mode is stable while Mack's second mode enters the growth zone when Mode F and Mode S have almost identical phase velocities (synchronization). When the synchronization is finished (at about $Re = 1200$), all the discrete modes decay. Case 2 is similar to Case 1 except the first mode has an unstable section due to wall-heating. The second mode, on the contrary, is stabilized by manifesting in a reduced overall growth rate.

The new mode appears in Case 3. One can still identify the Mode F and Mode S. However, Mode F synchronizes with the fast acoustic wave at a much larger Reynolds number. Synchronization between Mode F and Mode S still caused localized peak values of α_i for each other. Apparently, both modes are far from the unstable half-plane. Interestingly, the spectrum branching occurs indicating Mack's second mode has similar dispersion relation in this case. The new mode seems to stem from the vorticity/entropy wave ($c = 1.0$) and remains a phase velocity slightly larger than 1.0. At $Re = 1826$, the new mode becomes unstable and gains maximum growth rate at $Re = 3090$.

We pick the parameter of the (quasi-) most amplified new mode from Case 3 and plot the eigenvector of the new mode in Figure 5. Reynolds number $Re = 2000$, $\omega = 0.6$ and $\beta = 0$. The base flow is plotted as a reference. The boundary layer can be qualitatively divided into three regions shown in the figure. Region (1) starts from

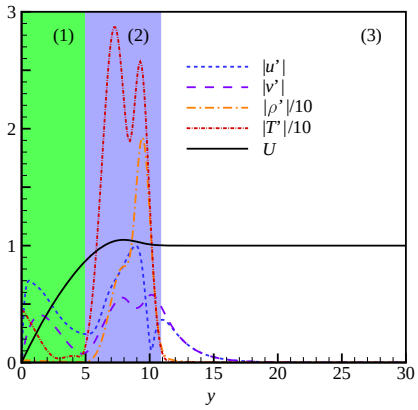

Figure 5. Eigenvector of the new mode at $Re = 2000$, $\omega = 0.6$ and $\beta = 0$. Absolute values are shown. The temperature and density perturbations are scaled with a factor of 0.1.

the wall and is replaced by Region (2) where the overshoot $U(y) > 1$ starts. Region (3) is the inviscid region outside the boundary layer.

The perturbations are mainly distributed in Region (1) and (2) where the baseflow shear exists. As expected in most hypersonic cases, temperature perturbation has the maximum amplitude, followed by the density components. Both perturbations are largely distributed in Region (2). The velocity perturbation $\tilde{u}$ and $\tilde{v}$ though have much smaller amplitudes but are critical for the transportation of momentum and energy of the fluids.

4 Concluding remarks

Inspired by Tunney *et al.* (2015), the viscous instability of the high-speed boundary layer with the dual effects of FPG and wall-heating is studied. From modal stability analysis, the full stability diagram (in the coordinates of $Re - \beta - \omega$) is given and compared with conventional first mode and Mack's second mode. The new mode becomes the only unstable modes in such flows where FPG readily suppressed the conventional modes. The synchronization between the spectrum found in high-speed flows (Federov & Tumin, 2011) remains but is not responsible for the growth of the new mode.

Acknowledgement

The authors acknowledge the financial support by the National Natural Science Foundation of China (Grant Nos. 11572176 and 11602127) and China Postdoctoral Science Foundation (No. 2016M590091).

REFERENCES

Bech, Knut H., Henningson, Dan S. & Henkes, Ruud A. W. M. 1998 Linear and nonlinear development of localized disturbances in zero and adverse pressure gradient boundary-layers. *Physics of Fluids* **10** (6), 1405–1418.

Cebeci, Tuncer 2002 *Convective heat transfer*. Springer.

Cebeci, Tuncer & Smith, A. M. O. 1974 *Analysis of turbulent boundary layers*. Academic Press.

Costantini, Marco, Hein, Stefan, Henne, Ulrich, Klein, Christian, Koch, Stefan, Schojda, Lukas, Ondrus, Vladimir & Schröder, Wolfgang 2016 Pressure gradient and nonadiabatic surface effects on boundary layer transition. *AIAA Journal* **54** (11), 3465–3480.

Federov, Alexander & Tumin, Anatoli 2011 High-speed boundary-layer instability: Old terminology and a new framework. *AIAA Journal* **49** (8), 1647–1657.

Fedorov, Alexander 2011 Transition and stability of high-speed boundary layers. *Annual Review of Fluid Mechanics* **43**, 79–95.

Fedorov, Alexander, Soudakov, Vitaly, Egorov, Ivan, Sidorenko, Andrey, Gromyko, Yury, Bountin, Dmitry, Polivanov, Pavel & Maslov, Anatoly 2015 High-speed boundary-layer stability on a cone with localized wall heating or cooling. *AIAA Journal* **53** (9), 2512–2524.

Franko, Kenneth J. & Lele, Sanjiva 2014 Effect of adverse pressure gradient on high speed boundary layer transition. *Physics of Fluids* **26** (2), 176–183.

Kloker, M. & Fasel, H. 1990 *Numerical Simulation of Two- and Three-Dimensional Instability Waves in Two-Dimensional Boundary Layers with Streamwise Pressure Gradient*, pp. 681–686. Berlin, Heidelberg: Springer Berlin Heidelberg.

Mack, Leslie M 1984 Boundary-layer linear stability theory. *Special Course on Stability and Transition of Laminar Flow, AGARD-R-709* .

Mack, Leslie M. 1987 *Review of Linear Compressible Stability Theory*, pp. 164–187. New York, NY: Springer New York.

Malik, Mujeeb R 1989 Prediction and control of transition in supersonic and hypersonic boundary layers. *AIAA Journal* **27** (11), 1487–1493.

Masad, Jamal A & Zurigat, Yousef H 1994 Effect of pressure gradient on first mode of instability in compressible boundary layers. *Physics of Fluids* **6** (12), 3945–3953.

Reed, H L, Saric, W S & Arnal, D 1996 Linear stability theory applied to boundary layers. *Annual Review of Fluid Mechanics* **28**, 389–428.

Ren, Jie & Fu, Song 2014 Competition of the multiple Görtler modes in hypersonic boundary layer flows. *SCIENCE CHINA Physics, Mechanics & Astronomy* **57** (6), 1178–1193.

Ren, Jie & Fu, Song 2015 Secondary instabilities of Görtler vortices in high-speed boundary layer flows. *Journal of Fluid Mechanics* **781**, 388–421.

Ricco, Pierre, Tran, Duc-Luan & Ye, Ganda 2009 Wall heat transfer effects on Klebanoff modes and Tollmien–Schlichting waves in a compressible boundary layer. *Physics of Fluids* **21** (2), 024106.

Saric, William S 1994 Görtler vortices. *Annual Review of Fluid Mechanics* **26**, 379–409.

Saric, William S., Reed, Helen L. & White, Edward B. 2003 Stability and transition of three-dimensional boundary layers. *Annual Review of Fluid Mechanics* **35**, 413–440.

Schlichting, Hermann & Gersten, Klaus 2017 *Boundary-Layer Theory*. Berlin, Heidelberg: Springer Berlin Heidelberg.

Tokugawa, Naoko, Choudhari, Meelan, Ishikawa, Hiroaki, Ueda, Yoshine, Fujii, Keisuke, Atobe, Takashi, Li, Fei, Chang, Chau Lyan & White, Jeffery 2015 Pressure gradient effects on supersonic transition over axisymmetric bodies at incidence. *AIAA Journal* **53** (12), 3737–3751.

Tunney, Adam P, Denier, James P, Mattner, Trent W & Cater, John E 2015 A new inviscid mode of instability in compressible boundary-layer flows. *Journal of Fluid Mechanics* **785**, 301–323.

Zhong, Xiaolin & Wang, Xiaowen 2012 Direct numerical simulation on the receptivity, instability, and transition of hypersonic boundary layers. *Annual Review of Fluid Mechanics* **44**, 527–561.

Zurigat, YH, Nayfeh, AH & Masad, JA 1992 Effect of pressure gradient on the stability of compressible boundary layers. *AIAA Journal* **30** (9), 2204–2211.